Volume 19, Number 3, 2026. pp. 343-353

Jordan Journal of Physics

ARTICLE

# Impact of Alkaline Conditions on the Properties and Stability of Zinc Oxide Nanoparticles Prepared via Green Synthesis for Thin Film Deposition

**Safiya J. Piro**[a], **Shaida A. Kakil**[b], **Mahira M. Esmael**[b], **Hunar Y. Muhammad**[c] and **Farhad Z. Ahmed**[b]

[a] *Department of Chemistry, Faculty of Science, Soran University, Erbil 44008, Kurdistan Region, Iraq.*

[b] *Department of Physics, College of Science, Salahaddin University-Erbil, Erbil, Kurdistan Region, Iraq.*

[c] *Department of Chemistry, College of Science, Salahaddin University-Erbil, Erbil, Kurdistan Region, Iraq.*

***DOI:*** **https://doi.org/10.47011/19.3.6**

*Received on: 26/06/2025;* *Accepted on: 02/10/2025*

**Abstract:** This study investigates the influence of pH on the properties and stability of ZnO nanoparticles synthesized via an eco-friendly process using fresh parsley. The research examines how pH variations during synthesis affect the structural, optical, and stability characteristics of ZnO nanoparticles. The findings show that increasing the pH shifts the band gap toward the blue region of the spectrum, expanding from 3.271 eV at pH 8 to 3.625 eV at pH 12. This shift suggests enhanced optical properties and greater stability at higher pH levels. Characterization using scanning electron microscopy and energy-dispersive X-ray spectroscopy confirmed a uniform nanoparticle structure and consistent elemental composition. Fourier-transform infrared spectroscopy verified the presence of ZnO functional groups, while X-ray diffraction analysis revealed a prominent peak at (002) at pH 12, indicating improved crystallinity at elevated pH levels. These findings offer valuable insights into optimizing green synthesis techniques for ZnO nanoparticles, contributing to advancements in nanotechnology and materials science. Furthermore, they provide a foundation for future studies on the long-term stability of these nanoparticles, particularly in thin-film applications, where pH-dependent effects may influence performance over time. The results show that the produced ZnO films have outstanding structural and optical properties, making them ideal as transparent conducting oxide layers. Their exceptional transparency and conductivity demonstrate their strong potential for use in solar energy and photovoltaic applications.

**Keywords:** ZnO nanoparticle, pH level, Stability, Green synthesis, Spin coating.

## 1. Introduction

Zinc oxide nanoparticles (ZnO) stand out among the numerous nanomaterials because of their exceptional characteristics, including a large surface area [1], optical clarity [2], and biocompatibility [3]. ZnO NPs possess properties that render them highly favorable for utilization in medication delivery, sensing, catalysis, and various other applications [4–7]. ZnO is an n-type, multifunctional semiconductor, with a higher exciton binding energy at room temperature (60 meV) than GaN and a direct bandgap energy of around 3.37 eV [8, 9]. Moreover, ZnO is known for its higher light transmittance and resistance to hydrogen plasma, which is frequently employed in manufacturing silicon-based photovoltaic devices [10]. Zinc oxide's high theoretical capacity, affordability, abundance, and

**Corresponding Author:** Shaida Anwar Kakil **Email**: shaida.kakil@su.edu.krd

environmental friendliness make it a viable anode material for Li-ion batteries [11, 12].

ZnO is a well-studied nanomaterial used in solar cells, UV light emitters, sensors, and piezoelectric nanogenerators. It also exhibits antibacterial, anticancer, antidiabetic, and antioxidant properties. Numerous synthesis techniques have been documented, including chemical precipitation, hydrothermal, sol-gel, spray pyrolysis, photochemical, green synthesis, and electrospinning. Recent studies have placed greater emphasis on green synthesis approaches as safer, more sustainable alternatives to conventional methods, which often require energy-intensive procedures and hazardous chemicals.us chemicals.

Green synthesis of ZnO nanoparticles involves the use of eco-friendly techniques that make use of natural resources like plant extracts, microbes [24], and biodegradable materials [25]. The process of green production of ZnO nanoparticles utilizes plant extracts from several plant species, which include distinct phytochemicals that serve as both reducing and stabilizing agents. Lolly Maria Jose et al. [26] produced ZnO nanoparticles using Aloe Vera extract and investigated the effectiveness of these nanoparticles in degrading malachite green, both with and without sunshine. They investigated the adsorption mechanism and predicted the adsorption rate [26]. Moringa Oleifera extract was used as a chelating agent to create ZnO nanocrystals, which were then analyzed for their morphology, structure, optical properties, and electrochemical activity [27]. Sharma et al. reported the green synthesis of triangular ZnO nanoparticles (G-ZnO NPs) using Azadirachta indica leaf extract and performed a shape-dependent density functional investigation for ZnO NPs on their antimicrobial activity [28]. Additionally, numerous studies have utilized various plants for synthesizing nanoparticles, such as tea, neem and coffee [13, 29–32]. The characteristics of synthesized metal oxide nanoparticles, such as ZnO and NiO, are significantly affected by precursor concentration and solution pH [13, 33]. It was also shown that pH significantly affects the photocatalytic and electrochemical activity of prepared nanoparticles. Furthermore, the production of ZnO nanoparticles using plant extracts, like parsley, has been investigated, emphasizing the role of pH in regulating nanoparticle properties and boosting photocatalytic activity [33].

The goal of this research is to synthesize zinc oxide nanoparticles (ZnO NPs) in an environmentally friendly manner and investigate their application in thin-film manufacturing under varied pH conditions. Fresh parsley extract was employed as a natural, cost-effective reducing and stabilizing ingredient to ensure a long-term synthesis process. To optimize nanoparticle formation, we conducted a comprehensive investigation into the effect of varied pH values (8–12) on the structural, morphological, and optical properties of ZnO particles. The produced nanoparticles were then coated as thin films using the spin-coating technique, allowing for a detailed examination of how synthesis conditions influence the properties of the resultant films, including morphology, elemental composition, vibrational properties, crystal structure, and optical properties. pH management is critical for manufacturing high-quality ZnO thin films because it influences nanoparticle development, shape, and surface properties. This study shows how pH tweaking of green-synthesized ZnO NPs can improve thin-film performance, providing insights into sustainable synthesis and furthering applications in optoelectronics and photovoltaics.

## 2. Materials and Experimental Setup

Zinc nitrate hexahydrate ($Zn(NO_3)_2 \cdot 6H_2O$) with a purity of 98.0% and sodium hydroxide pellets (NaOH) were acquired from Sigma-Aldrich. ZnO thin films were synthesized using fresh parsley. A 25-g sample of parsley leaves was thoroughly cleaned, cut into tiny pieces, combined with 100 mL of distilled water, and heated at 65°C for 40 minutes. The resulting aqueous extract was filtered, centrifuged at 5000 revolutions per minute for 20 minutes, and then stored in the refrigerator for future use. Zinc oxide (ZnO) nanoparticles were synthesized by slowly adding 50 mL of parsley extract to 50 mL of zinc nitrate hexahydrate ($Zn(NO_3)_2 \cdot 6H_2O$) while stirring with a magnetic stirrer at a temperature of 80°C for 2 hours. The pH of the mixture was adjusted to 8, 10, and 12 by introducing sodium hydroxide (NaOH) (Fig. 1). No additional stabilizing agents were used, as the parsley extract's phytochemicals (O–H, C=O, C–O groups) naturally act as reducing and capping agents. The spin coating technique was

employed for 30 seconds at a rotational speed of 3000 revolutions per minute at ambient temperature. The resulting film was then heated to 200°C ± 5°C for 5 minutes. The coating procedure was repeated three times to produce films with uniform composition (Fig. 2). XRD measurements were performed using a Rigaku C/max-2500 diffractometer with Cu Kα radiation (λ = 1.5406 Å) at an applied voltage of 40 kV and a current of 30 mA. The chemical composition was analyzed using Fourier transform infrared spectroscopy (FTIR; IRAffinity-1S) in the mid-infrared range of 400–4000 $cm^{-1.}$ The optical properties were measured using a Shimadzu UV-1800 UV-visible spectrophotometer that operates in the wavelength range of 190–1100 nm. The surface morphology of the films was evaluated using scanning electron microscopy (SEM; CamScan MV2300). The chemical composition of the deposited films was analyzed by energy-dispersive X-ray spectroscopy (EDS).

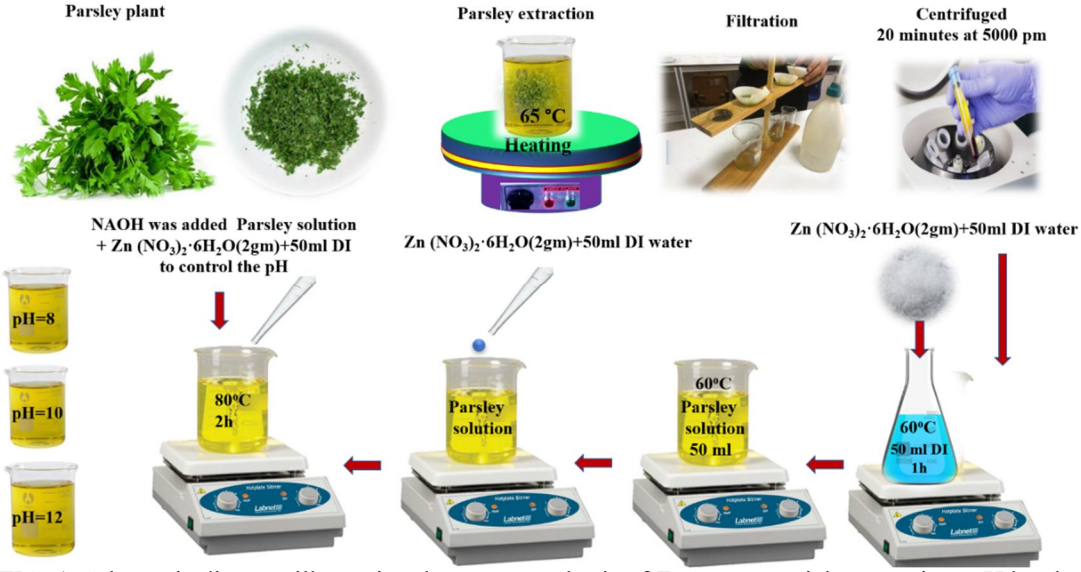


FIG. 1. Schematic diagram illustrating the green synthesis of ZnO nanoparticles at various pH levels.

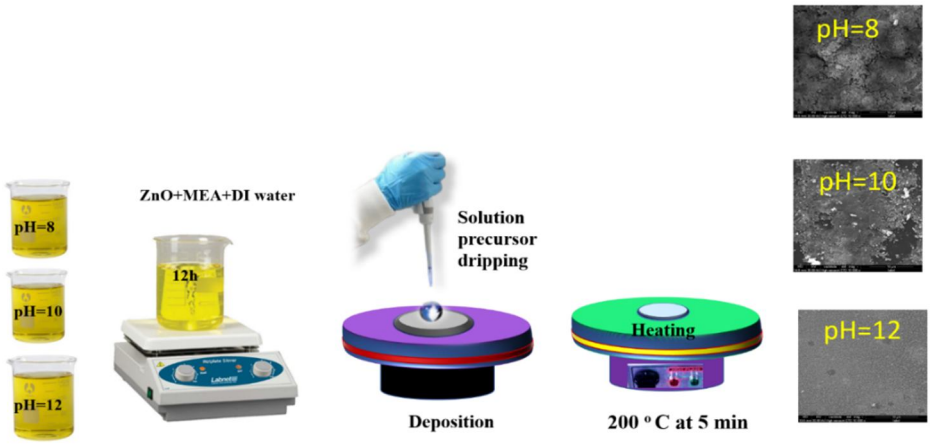


FIG. 2. Schematic diagram illustrating the deposition of ZnO nanoparticles on Si and glass by spin coating at various pH levels.

## 3. Results and Discussions

### *3.1 UV-Visible Spectroscopy and Stability*

The UV-visible absorption spectra of ZnO nanoparticle colloidal solutions prepared at pH 8, 10, and 12 show distinct absorption bands. As shown in Fig. 3, at pH 8, the material exhibits an absorption band at 379 nm, which agrees well with literature reports in the wavelength range of 310 nm to 378 nm [34, 35]. Raising the pH to 10 causes a blue shift, with the band-gap absorption shifting to 368 nm, indicating a change in electronic structure or particle size. Raising the pH to 12 causes a further blue shift to 342 nm. This suggests additional changes in the band gap and possibly changes in the shape or surface properties of the nanoparticles. Furthermore, at pH 12, the absorption band

shows significantly higher intensity, indicating improved light-absorption abilities that may be associated with a higher density or homogeneity of nanoparticles in the colloidal solution. The results emphasize that pH is a critical factor that affects both the wavelength and intensity of absorption in ZnO nanoparticles. Furthermore, Arokiyadoss and Rayerfrancis et al. [36] found that UV absorbance by ZnO is affected by pH. They observed that as the precursor solutions shifted from acidic to neutral and basic conditions, the absorbance intensity in the UV region gradually increased. The observed pattern indicates that ZnO nanostructures produced in a pH-neutral environment possess a very crystalline structure.

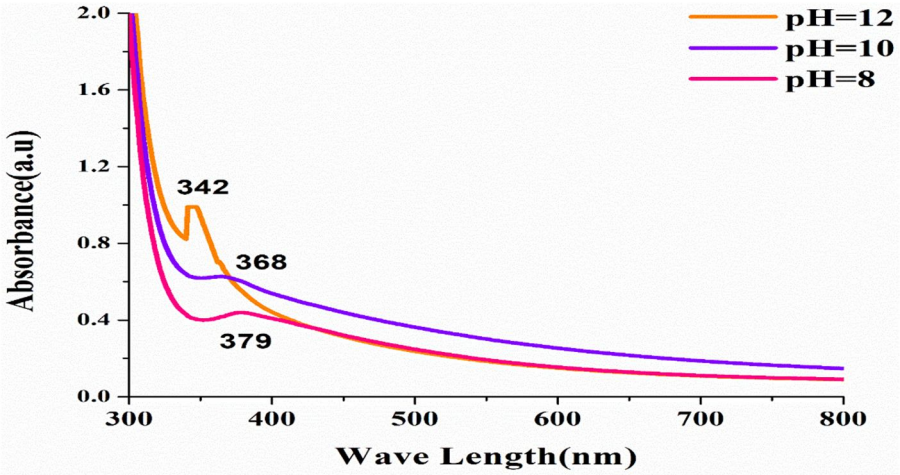


FIG. 3. UV-visible absorption spectra of the colloidal solution of ZnO NPs on glass prepared at different pH values (8, 10, and 12).

Figure 4 shows the UV-visible spectra of colloidal ZnO nanoparticles at different pH levels, illustrating how pH affects their aggregation characteristics. Table 1 summarizes the UV-visible absorption bands and band gap edges detected during the growth process and after three months of storage under ambient conditions. The decrease in the band gap edge observed after three months is related to agglomeration of nanoparticles. At pH 12, the nanoparticles show greater stability in comparison to lower pH values. They show little change in both the position and strength of their absorption band over the same duration. This suggests that pH significantly affects the stability and optical characteristics of the ZnO nanoparticles. Specifically, alkaline environments promote greater stability against aggregation.

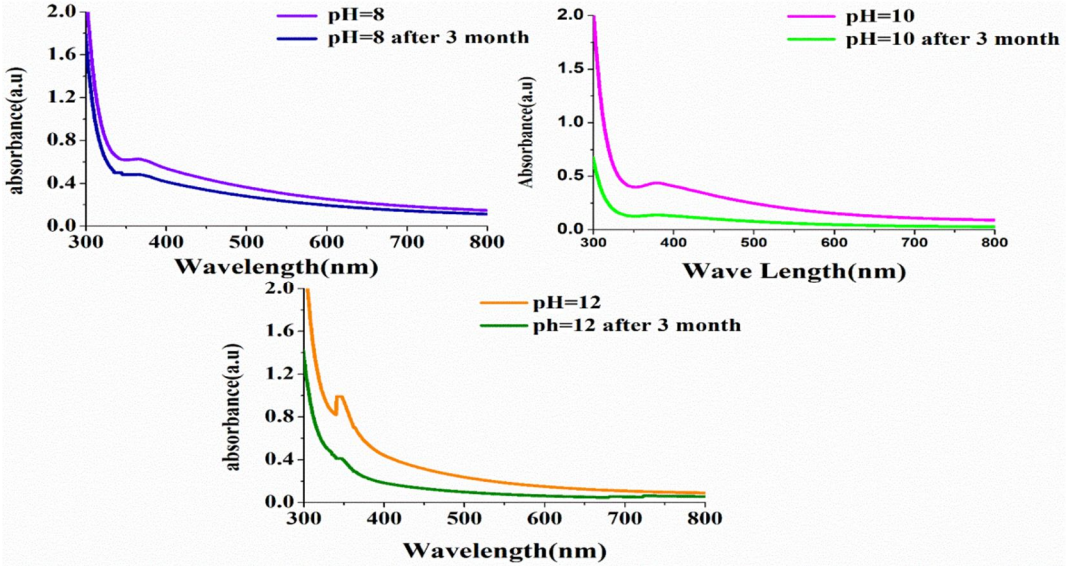


FIG. 4. Stability of colloidal ZnO nanoparticles analyzed by UV-visible spectrophotometry at different pH levels (8, 10, and 12) during growth and after three months.

TABLE 1. UV-Visible absorption bands and band gap edges observed during the growth process and after 3 months at different pH values.

| pH Level | Absorption Peak (During Growth) (nm) | Band gap edge (eV) | Absorption Band (After 3-Month Period) (nm) | Band gap edge (eV) |
|---|---|---|---|---|
| 8 | 379 | 3.271 | …… | …… |
| 10 | 368 | 3.369 | …… | …… |
| 12 | 342 | 3.625 | 348 | 3.563 |

*3.2 Morphology and Compositional Analysis*

Figure 5 represents SEM images of prepared ZnO NPs. At low magnification, the SEM image shows irregular ZnO nanostructures that are less uniform in shape and distribution. The nanostructures appear to be more amorphous or less crystalline, possibly because the slightly alkaline pH can influence the nucleation and growth of ZnO particles. At higher magnification (left side in Fig. 5a), the ZnO structures appear smaller and may exhibit some aggregation or clustering. This suggests that at pH 8, the growth of ZnO is slower and less controlled, resulting in a less organized morphology. At pH 10, the SEM images show a more uniform surface with well-distributed ZnO nanostructures. This pH appears to favor the synthesis of more homogeneous and well-formed ZnO structures. The material at this pH likely exhibits more defined nanostructures. The higher crystallinity and more regular morphology at pH 10 indicate that this pH range promotes optimal growth and deposition, leading to a better-formed structure with fewer defects. At pH 12, the SEM images show a denser, more compact structure with larger ZnO particles or agglomerates. The surface appears rougher compared to the pH 10 sample, which may be due to the accelerated growth rate at higher pH. This pH condition likely leads to larger particle formation or greater aggregation during the synthesis process. At higher magnification, the ZnO particles may show more significant aggregation, indicating that at higher pH the growth process was faster and resulted in irregular or larger clusters of ZnO. Previous studies have focused on how pH affects the morphology of ZnO nanostructures. For example, M. Jay Chithra et al. [37] used a chemical precipitation method to investigate the impact of pH on the dimensions and morphology of zinc oxide nanoparticles. In contrast, our study utilizes green synthesis followed by spin-coating, and we explore the effect of pH on the dispersion homogeneity of ZnO nanostructures under different conditions.

Figure 6 shows the particle size distribution of zinc oxide nanostructures prepared at pH = 12, as assessed with ImageJ software based on the SEM image displayed in the inset. The histogram shows that the ZnO nanoparticles range in size from about 35 to 95 nm, with the majority of particles localized between 55 and 70 nm. The Gaussian fit shows a reasonably narrow distribution, verifying the homogeneity of the produced nanoparticles. The SEM image provides direct visual evidence of the nanostructures' shape and confirms their nanoscale dimensions. The prevalence of particles within this range indicates that the alkaline medium (pH = 12) enabled regulated nucleation and development, resulting in ZnO nanoparticles with enhanced homogeneity.

Figure 7 represents the EDX spectra of zinc oxide nanostructures prepared under different pH settings. The spectra show clear peaks that correlate with the elemental makeup of the nanostructures, with clear detection of zinc and oxygen. Furthermore, the spectra exhibit distinct silicon peaks, which can be ascribed to the utilization of a silicon substrate in the synthesis procedure. The EDX spectra reveal changes in elemental composition, providing significant information about how the pH affects the structural features of the produced zinc oxide nanostructures. Table 2 presents the EDX atomic percentage of the zinc oxide nanostructures synthesized at different pH conditions. The atomic percentages of zinc (Zn) and oxygen (O) closely match the stoichiometric composition of ZnO (1:1).

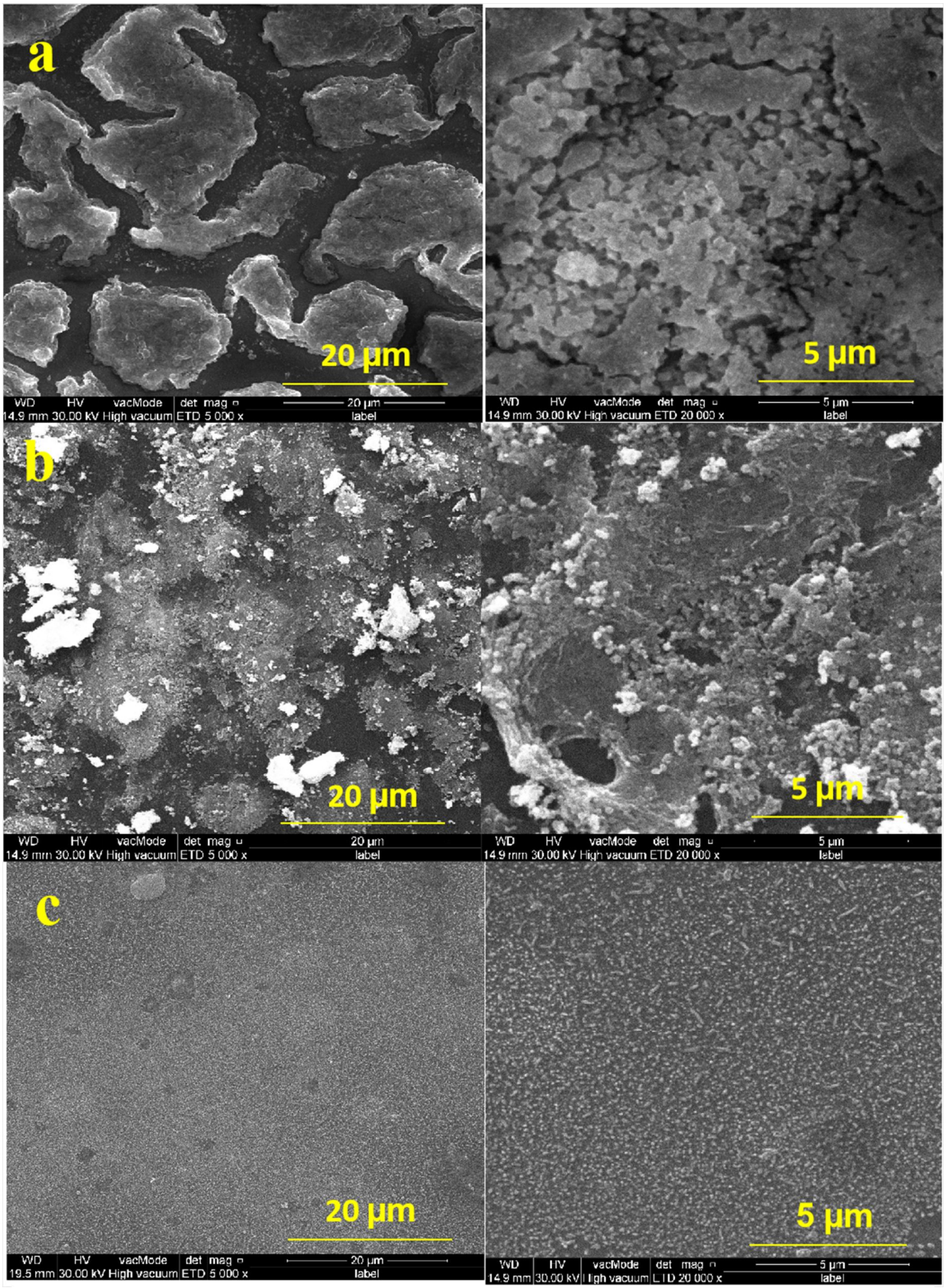


FIG. 5. SEM images provide visual insight into zinc oxide nanostructures synthesized using green synthesis techniques under varying pH conditions: a: pH=8, b: pH=10, and c: pH=12.

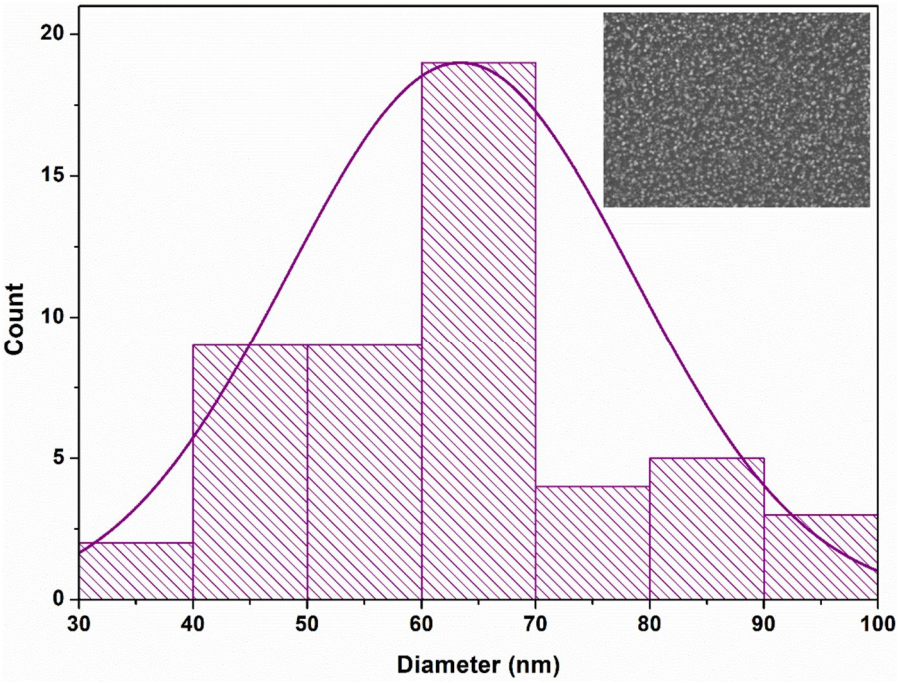


FIG. 6. Size distribution of ZnO nanoparticles prepared at pH = 12.

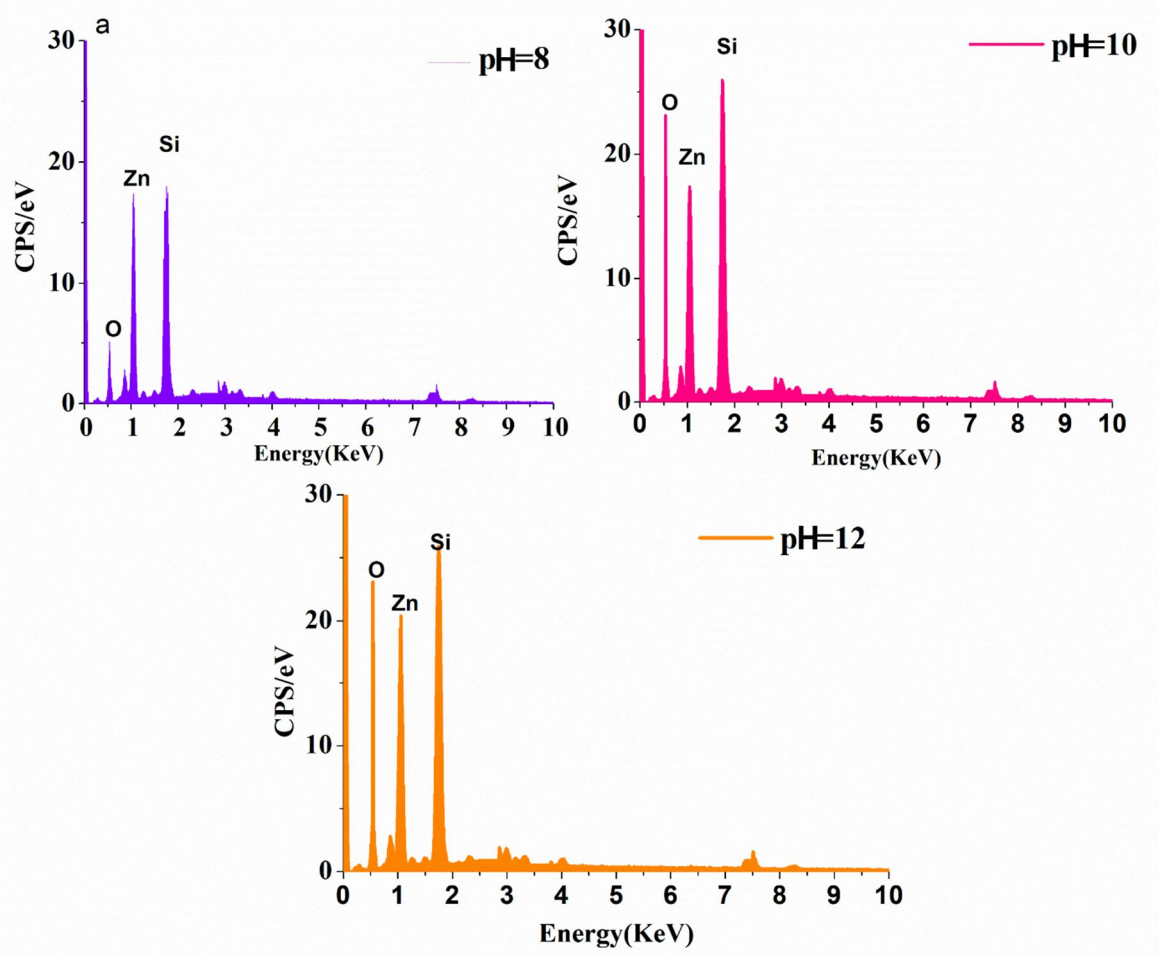


FIG. 7. EDX spectra of Zinc oxide nanostructures synthesized at different pH conditions.

TABLE 2. EDX atomic percentage of Zinc oxide nanostructures synthesized at different pH conditions.

| Elements | pH 8 Atomic % | pH10 Atomic % | pH12 Atomic % |
|---|---|---|---|
| Silicon | 45.123 | 40.043 | 37.556 |
| Oxygen | 27.012 | 30.032 | 31.439 |
| Zinc | 28.123 | 29.985 | 31.0123 |
| Zn/O | 1.0411 | 0.998 | 0.986 |

*3.3 Structural Analysis*

Figure 8 displays the XRD patterns of the prepared ZnO nanostructures on glass at all three pH levels. The observed patterns are in agreement with the hexagonal wurtzite structure, with distinct high-intensity peaks related to the (100), (002), and (101) planes, most prominent at pH 12. Similarly, the peak corresponding to the (100) plane was obvious at pH 10. These findings indicate the formation of the wurtzite phase of ZnO (JCPDS # 89-1397) under applied conditions. The XRD patterns were used to estimate crystallite size using the Scherrer formula. No discernible peaks were observed at pH 8, indicating an amorphous structure. At pH 10, a peak was observed at 31.545°. This peak corresponds to a crystallite size of 30.728 nm. At pH 12, diffraction peaks appear at 31.545°, 34.242°, and 36.004°. The corresponding crystallite sizes were determined to be 17.600 nm, 26.526 nm, and 26.526 nm, respectively, as shown in Table 3. The findings demonstrate that pH significantly impacts the crystallization of ZnO nanostructures. At pH 8, the lack of distinct peaks suggests an amorphous state due to insufficient $OH^-$ concentration. In contrast, at higher pH levels (10 and 12), ZnO shows sharper peaks, indicating better crystallinity. The decrease in crystallite size with increasing pH from pH 8 to 12 suggests improved nucleation and crystallization, leading to smaller and more ordered ZnO crystals. This underscores the critical role of pH in shaping the structural properties of ZnO nanostructures.

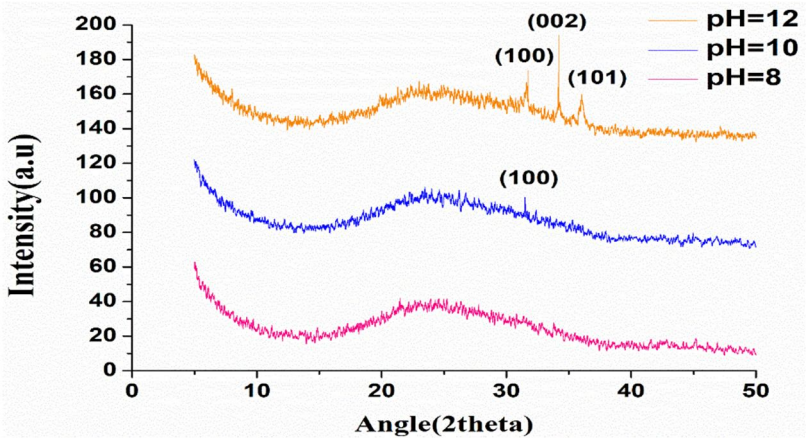


FIG. 8. XRD of ZnO nanostructures prepared at various pH conditions.

TABLE 3. Estimation of crystallite size from XRD data for varied pH conditions.

| pH | Position (2 Theta) | Crystallite size D (nm) |
|---|---|---|
| 8 | no | no |
| 10 | 31.545 | 30.728 |
| 12 | 31.545 | 17.600 |
| 12 | 34.242 | 26.526 |
| 12 | 36.004 | 26.526 |

*3.4 Vibrational Properties*

Figure 9 shows the FTIR spectra of prepared ZnO nanostructures. At pH 8, the O-H stretching vibration appears at a wavenumber of 3338 $cm^{-1}$, slightly shifting to 3325 $cm^{-1}$ and 3300 $cm^{-1}$ upon increasing the pH to 10 and 12, respectively. As pH increases, there is a growing contact between the hydroxide groups and the ZnO nanostructures. The band at 1632-1646 $cm^{-1}$ is attributed to the bending vibration of water

(moisture contained in the sample). This band around 640-660 $cm^{-1}$ is most probably due to $Zn(OH)_2$ accompanied by some contribution of C-H bending from the organic residue of the parsley extract. The absorption features around 600 $cm^{-1}$ are attributed to Zn-O [38, 39]. In agreement with literature reports [38], another Zn-O vibration is observed at 460 $cm^{-1}$ for pH 8, 457 $cm^{-1}$ for pH 10, and 418 $cm^{-1}$ for pH 12. The modest frequency shift may reflect changes in crystallinity and bonding in the ZnO nanostructures across pH values. The decrease in the wavenumber of Zn-O vibrations in FTIR spectra with decreasing ZnO nanoparticle size is attributed to quantum confinement effects and modifications in surface properties, as suggested by Qiao et al. [40]. The remaining phytochemicals from the parsley extract, which serve as capping and stabilizing agents, have another significant impact. These molecules, which have O–H, C=O, and C–O functional groups, interact with $Zn^{2+}$ ions to change the local chemical environment and cause minor shifts or broadening of the Zn–O bands [41, 42]. Furthermore, smaller ZnO nanoparticles are formed at higher pH, encouraging faster nucleation rates.

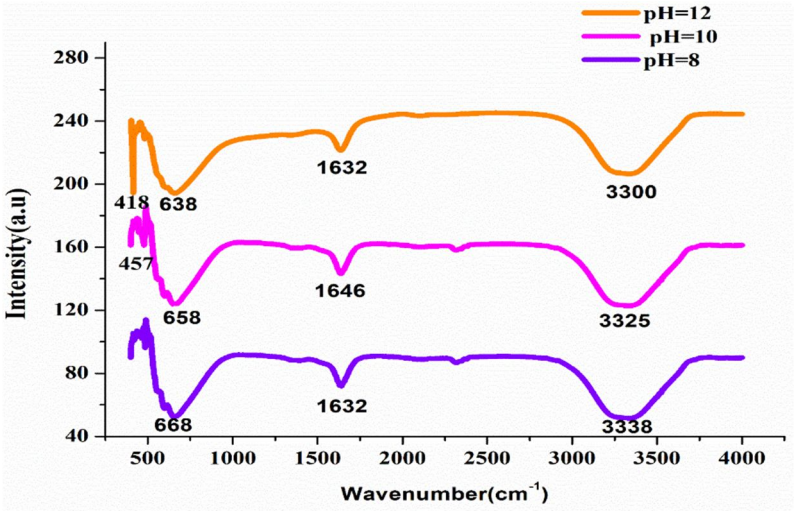


FIG. 9. FTIR spectra of zinc oxide nanostructures prepared at various pH conditions.

## 4. Conclusion

This study successfully demonstrates the synthesis and characterization of ZnO nanoparticles using green synthesis methods, specifically incorporating parsley extract at various pH levels. Zinc nitrate hexahydrate and sodium hydroxide were employed to produce ZnO thin films and nanoparticles at pH 8, 10, and 12. The synthesis process, including spin coating and heat treatment, produced uniform, well-defined ZnO nanostructures. UV-visible spectroscopy revealed a blue shift in the absorption spectra as the pH increased from 8 to 12, indicating changes in the band gap and enhanced optical properties at higher pH levels. Absorption intensity also increased with pH, suggesting improved light absorption. Stability tests showed that ZnO nanoparticles synthesized at pH 12 exhibited slightly better stability over time compared to those produced at lower pH values. SEM revealed that higher pH levels produced smaller, more homogeneous ZnO nanoparticles with a more uniform particle size distribution. XRD confirmed the formation of the hexagonal wurtzite structure, with improved crystallinity at pH 12. FTIR confirmed pH-dependent changes in functional groups. The results show that pH is essential for adjusting the stability, optical, and structural characteristics of ZnO nanostructures. Importantly, the optimized ZnO nanoparticles and thin films produced at high pH levels have a lot of potential for use in solar cells, gas sensors, and UV-photodetector applications where improved stability, optical absorbance, and crystallinity are highly desired.

## Acknowledgments

The authors would like to express their gratitude to the Department of Physics Education at Soran University for providing the equipment and supplies essential for preparing and characterizing the samples used in this study. They also sincerely acknowledge the support and facilities offered by the College of Science,

Department of Physics, Salahaddin University-Erbil, which played a crucial role in the successful completion of this study.

**Funding**: No funding was provided.

**Conflict of Interests**

The authors confirm that there are no conflicts of interest.

**Author Contributions**

Safiya Jameel Piro: Conceptualization, Investigation, Formal analysis; Shaida Anwer Kakil: Conceptualization, Visualization, Validation, Writing-review & editing, Resources and Supervision; Mahira Muhsen Esmael: Formal analysis, Validation, Writing—review & editing; Hunar Yasin Muhammad and Farhad Zrar Ahmed: Software, Validation, review & editing.

**References**

[1] Rustembekkyzy, K., Sabyr, M., Kanafin, Y.N., Khamkhash, L., and Atabaev, T.S., RSC Advances, 14 (2024) 16293.

[2] Gadewar, M. et al., Journal of Saudi Chemical Society, 28 (2024) 101774.

[3] Ashour, M.A. and Abd-Elhalim, B.T., Scientific Reports, 14 (2024) 4147.

[4] Hassan, Y.M. and Kakil, S.A., Journal of Materials Science: Materials in Electronics, 26 (2015) 6092.

[5] Aziz, F.F.A., Timmiati, S.N., Jalil, A.A., Rusdan, N.A., Annuar, N.H.R., and The, L.P., Journal of Environmental Chemical Engineering, 12 (2024) 112976.

[6] Anjum, S., Hashim, M., Malik, S.A., Khan, M., Lorenzo, J.M., Abbasi, B.H., and Hano, C., Cancers, 13 (2021) 4570.

[7] Al-Rawashdeh, N.A.F., Allabadi, O., and Aljarrah, M.T., ACS Omega, 5 (2020) 28046.

[8] Klingshirn, C., Hauschild, R., Fallert, J., and Kalt, H., Physical Review B—Condensed Matter and Materials Physics, 75 (2007) 115203.

[9] Henini, M., "Molecular Beam Epitaxy: From Research to Mass Production", 2nd ed., (Elsevier, 2018), 343–375, Chapter 16.

[10] Khan, I.H., "Nanomaterials for Innovative Energy Systems and Devices", (Springer, 2022), 173–241, Chapter 6.

[11] Kim, H., Jae, W., Song, J., and Kim, J., Journal of Alloys and Compounds, 772 (2019) 507.

[12] Awasthi, K., "Nanostructured Zinc Oxide", (Elsevier, 2021), 575–603, Chapter 6.

[13] Purushotham, D., Mavinakere Ramesh, A., Shetty Thimmappa, D., Kalegowda, N., Hittanahallikoppal Gajendramurthy, G., Kollur, S.P., and Mahadevamurthy, M., International Journal of Molecular Sciences, 26 (2025) 1.

[14] Song, D., Aberle, A.G., and Xia, J., Applied Surface Science, 195 (2002) 291.

[15] Abdelghany, T.M., Al-Rajhi, A.M.H., Yahya, R., Bakri, M.M., Al Abboud, M.A., Yahya, R., Qanash, H., Bazaid, A.S., and Salem, S.S., Biomass Conversion and Biorefinery, 13 (2023) 417.

[16] Lim, Y.P., Koay, J.S.C., Zhao, J., Huang, S., Goh, B.T., Aw, K.C., Chen, B., Haw, C.Y., and Gan, W.C., Advanced Functional Materials, 32 (2022) 2206750.

[17] Park, Y.J., Song, H., Ko, K.B., Ryu, B.D., Cuong, T.V., and Hong, C.-H., Journal of Nanomaterials, 2016 (2016) 7947623.

[18] Mandal, A.K., Katuwal, S., Tettey, F., Gupta, A., Bhattarai, S., Jaisi, S., Bhandari, D.P., Shah, A.K., Bhattarai, N., and Parajuli, N., Nanomaterials, 12 (2022) 3066.

[19] Xiao, D., Wang, Y., Zhang, D., Liu, Y., Wang, H., Li, Y., Wei, H., Wang, S., Sun, M., and Sun, M., Ceramics International, 50 (2024) 15767.

[20] Di Mauro, A., Zimbone, M., Fragalà, M.E., and Impellizzeri, G., Materials Science in Semiconductor Processing, 42 (2016) 98.

[21] Rajan, S., Venugopal, A., Kozhikkalathil, H., Valappil, S., Kale, M., Mann, M., Ahuja, P., and Munjal, S., Materials Today: Proceedings (2023).

[22] Bulcha, B., Leta Tesfaye, J., Anatol, D., Shanmugam, R., Dwarampudi, L.P., Nagaprasad, N., Bhargavi, V.L.N., and Krishnaraj, R., Journal of Nanomaterials, 2021 (2021) 8617290.

[23] Alaserhat, İ., Yıldız, F., Karabiçak, Y., Seren, E., Gözüaçık, C., Tuncer, S., Bozkurt, A., Alıcı, H., Ataş, M., and Maral, V., Applied Fruit Science, 67 (2025) 1.

[24] Mohd Yusof, H., Mohamad, R., Zaidan, U.H., and Abdul Rahman, N.A., Journal of Animal Science and Biotechnology, 10 (2019) 57.

[25] Kalaba, M.H., El-Sherbiny, G.M., Ewais, E.A., Darwesh, O.M., and Moghannem, S.A., BMC Microbiology, 24 (2024) 254.

[26] Jose, L.M., Raj, R.S.A., Sajan, D., and Aravind, A., Nano Express, 2 (2021) 10039.

[27] Letsholathebe, D., Thema, F.T., Mphale, K., Maabong, K., and Maria Magdalane, C., Materials Today: Proceedings, 36 (2021) 475.

[28] Sharma, B.K., Mehta, B.R., Shah, E.V., Chaudhari, V.P., Roy, D.R., and Mondal Roy, S., Journal of Cluster Science, 1 (2022) 1.

[29] Abel, S., Tesfaye, J.L., Shanmugam, R., Dwarampudi, L.P., Lamessa, G., Nagaprasad, N., Benti, M., and Krishnaraj, R., Journal of Nanomaterials, 2021 (2021) 3413350.

[30] Thi, T.U.D., Nguyen, T.T., Thi, Y.D., Thi, K.H.T., Phan, B.T., and Pham, K.N., RSC Advances, 10 (2020) 23899.

[31] Vieira, I.R.S., da Silva, A.A., da Silva, B.D., Neto, L.T., Tessaro, L., Furtado, C.R.G., de Sousa, A.M.F., Carvalho, N.M.F., and Conte-Junior, C.A., "Biomass Conversion and Biorefinery", (2023).

[32] Mohammadi, A., Hashemi, N., Ghassabzadeh, M., Sharafi, A., Yazdinezhad, A., and Danafar, H., Scientific Reports, 15 (2025) 20853.

[33] Aliannezhadi, M., Doost Mohamadi, F., Jamali, M., and Shariatmadar Tehrani, F., Scientific Reports, 15 (2025) 7203.

[34] Sasani Ghamsari, M., Alamdari, S., Han, W., and Park, H.-H., International Journal of Nanomedicine, 2017 (2017) 207.

[35] Pudukudy, M., and Yaakob, Z., Journal of Cluster Science, 26 (2014) 1.

[36] Rayerfrancis, A., Bhargav, P.B., Ahmed, N., Chandra, B., and Dhara, S., Physica B: Condensed Matter, 457 (2015) 96.

[37] Jay Chithra, M., Sathya, M., and Pushpanathan, K., Acta Metallurgica Sinica (English Letters), 28 (2015) 394.

[38] Maher, S., Nisar, S., Aslam, S.M., Saleem, F., Behlil, F., Imran, M., Assiri, M.A., Nouroz, A., Naheed, N., and Khan, Z.A., ACS Omega, 8 (2023) 15920.

[39] Patel, M., Mishra, S., Verma, R., and Shikha, D., Discover Materials, 2 (2022) 1.

[40] Qiao, H., Wei, Z., Yang, H., Zhu, L., and Yan, X., Journal of Nanomaterials, 2009 (2009) 795928.

[41] Ribut, S.H., Che Abdullah, C.A., Mustafa, M., Mohd Yusoff, M.Z., and Ahmad Azman, S.N., Materials Research Express, 6 (2019) 25016.

[42] Alias, S.S., Ismail, A.B., and Mohamad, A.A., Journal of Alloys and Compounds, 499 (2010) 231.